Mon. Not. R. Astron. Soc. **386,** 963–972 (2008) doi:10.1111/j.1365-2966.2008.13079.x

H I aperture synthesis and optical observations of the pair of galaxies NGC 6907 and 6908

S. Scarano Jr,[1⋆] Felipe R. H. Madsen,[2] Nirupam Roy[3] and J. R. D. Lépine[1]

[1]*Instituto de Astronomia, Geofísica e Ciências Atmosféricas da Universidade de São Paulo, Cidade Universitária 05508-900 São Paulo, SP, Brazil*
[2]*Instituto Nacional de Pesquisas Espaciais, Jd. Granja 12227-010, São José dos Campos, SP, Brazil*
[3]*NCRA-TIFR, Post Bag 3, Ganeshkhind, Pune 411 007, India*

Accepted 2008 February 6. Received 2008 January 30; in original form 2007 December 31

ABSTRACT

NGC 6908, an S0 galaxy situated in the direction of NGC 6907, was only recently recognized as a distinct galaxy, instead of only a part of NGC 6907. We present 21-cm radio synthesis observations obtained with the Giant Metrewave Radio Telescope (GMRT) and optical images and spectroscopy obtained with the Gemini-North telescope of this pair of interacting galaxies. From the radio observations, we obtained the velocity field and the H I column density map of the whole region containing the NGC 6907/8 pair, and by means of the Gemini multi-object spectroscopy we obtained high-quality photometric images and 5 Å resolution spectra sampling the two galaxies. By comparing the rotation curve of NGC 6907 obtained from the two opposite sides around the main kinematic axis, we were able to distinguish the normal rotational velocity field from the velocity components produced by the interaction between the two galaxies. Taking into account the rotational velocity of NGC 6907 and the velocity derived from the absorption lines for NGC 6908, we verified that the relative velocity between these systems is lower than 60 km s^{-1}. The emission lines observed in the direction of NGC 6908, not typical of S0 galaxies, have the same velocity expected for the NGC 6907 rotation curve. Some emission lines are superimposed on a broader absorption profile, which suggests that they were not formed in NGC 6908. Finally, the H I profile exhibits details of the interaction, showing three components: one for NGC 6908, another for the excited gas in the NGC 6907 disc and a last one for the gas with higher relative velocities left behind NGC 6908 by dynamical friction, used to estimate the time when the interaction started in $(3.4 \pm 0.6) \times 10^7$ yr ago.

Key words: galaxies: interactions – galaxies: kinematics and dynamics – galaxies: photometry – radio lines: galaxies.

1 INTRODUCTION

Searching for companions among the nearby barred galaxies from the Shapley–Ames Catalogue, García-Barreto, Carrillo & Vera-Villamizar (2003) identified NGC 6908 as a discoidal companion of NGC 6907, 10 kpc away from it. They estimated this distance based only on their angular separation. But according to these authors, the alignment of the objects could be a mere effect of geometrical superposition, as the narrow-band Hα images of NGC 6907 did not reveal any emission in the direction of NGC 6908 (García-Barreto et al. 1996). Surace, Sanders & Mazzarella (2004) recognized NGC 6907 and 6908 as a potential interacting system, but the low resolution of their far-infrared images did not allow any further conclusion.

In a recent paper, Madore et al. (2007) revealed that NGC 6908, once classified as a PofG (part of a galaxy), is in fact a lenticular S0(6/7) galaxy, as indicated by its exponential brightness profile observed in several filters. Based on long-slit observations, these authors found different radial velocities for NGC 6908 lines in absorption (3113 ± 73 km s^{-1}) and in emission (3060 ± 16) km s^{-1}. Comparing with the radial velocity that they estimated for NGC 6907 (3190 ± 5 km s^{-1}), the velocity difference between the two systems would be in the interval of 77 to 130 km s^{-1}. Summing the evidences of morphological asymmetry in the arm structure of NGC 6907, the behaviour of its dust lanes and the tail of debris observed at low surface brightness, they conclude that the two galaxies are certainly interacting.

Despite the convincing arguments in favour of the interacting nature of the two galaxies, one could still question whether the absorption and emission lines observed in the direction of NGC 6908 are indeed from that galaxy or originate from the rotating disc of NGC 6907. Studies of rotation curves of spiral galaxies based on ionized gas (emission lines) and on the stellar component (absorption lines) have shown that, for most galaxies, the rotation of the two components is similar, but local differences of velocities up

⋆E-mail: scarano@astro.iag.usp.br

to 100 km s^{-1} can occur (Saito et al. 1984; Fillmore, Boroson & Dressler 1986; Kormendy & Westpfahl 1989; Vega Beltrán et al. 2001; Pizzella et al. 2004; Rhee et al. 2004). On the other hand, only luminous S0 galaxies are expected to present detectable emission lines. Since NGC 6908 is a low-luminosity S0(6/7) galaxy ($M_B = -17.4$; Madore et al. 2007) superimposed on the spiral arm of NGC 6907, the lines used to measure its velocity could well originate in the rotating material of the disc of NGC 6907.

In this paper, we present new observations, at radio and optical wavelengths, that allow us to definitely settle this question, and to propose a scenario that describes in more detail the recent collision between the two galaxies. We performed high-resolution radio observations at 21 cm with the Giant Metrewave Radio Telescope (GMRT), and a detailed spectroscopic study over the field of the system NGC 6907 and 6908, with the Gemini-North telescope.

At 21 cm, using the aperture synthesis technique, the H I intensity maps and the velocity fields of both objects were obtained. The emission of the two objects could be distinguished and their velocities precisely measured. Furthermore, the excess in velocity in the velocity field was used to estimate the time passed from the start of the interaction.

The optical multi-object spectroscopy, employing the Gemini Multi-Object Spectrograph (GMOS) instrument, allowed the study of the emission and absorption lines of selected H II regions in the NGC 6907 disc and the nucleus of both galaxies. Each observed spectrum could be compared with its radio counterpart and the differences in absorption and emission velocities in the direction of NGC 6908 could be explained by the idea that the emission lines were generated on the NGC 6907 disc and the absorption lines were formed on NGC 6908.

2 THE FIELD OF NGC 6907/8

Inside a field of 24 × 24 arcmin^2 centred on NGC 6907 (Fig. 1), only two extragalactic objects dominate the optical emission: NGC 6907 itself, an SBbc spiral galaxy (Eskridge et al. 2002) with an absolute B magnitude $M_B = -21.34$ and a surface brightness of 22.29 mag arcsec^{-2} at half B total light (Lauberts & Valentijn 1989) and NGC 6908, an S0(6/7) galaxy with $M_B = -17.4$ (Madore et al. 2007), 43.6 arcsec north-west from NGC 6907. Garcia (1993) mentioned NGC 6907 as the main member of a sparse group of three galaxies (IC 4999 and 5005, without considering NGC 6908), also identified in the catalogue of galaxy groups of Maia, da Costa & Latham (1989), but these objects cannot be seen in the field shown in the figure. In the radio continuum at 1.4 GHz, NGC 6907 is also the brightest object, as can be seen in the National Radio Astronomy Observatories (NRAO) Very Large Array (VLA) Sky Survey (NVSS; Condon et al. 1998). The main properties of NGC 6907/8 galaxies are listed in Table 1.

3 GEMINI OBSERVATIONS

Optical observations were conducted at the Gemini-North telescope using the imaging and multislit spectroscopic capabilities of the GMOS in queue mode.

Before the observations, publicly available images of NGC 6907 were used to pre-select the best H II region candidates on it as well to determine the optimum position angle for the observation (243° or 63° – from north to east). This angle minimizes the number of selected objects that would have overlapping spectra on the GMOS detector.

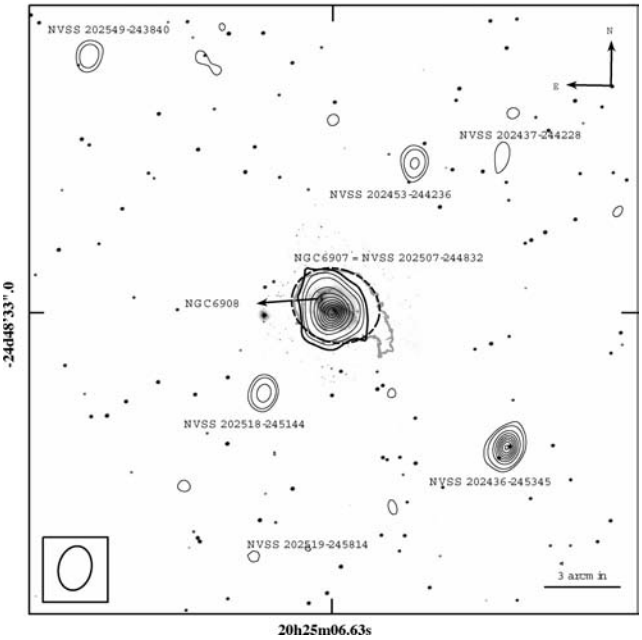

Figure 1. Optical image of the field centred in NGC 6907 galaxy and covering 24 × 24 arcsec^2. It is overlaid by the GMRT continuum observation. The contours are associated with the levels 2, 4, 11, 18, 25, 33, 40, 47, 54 and 61 mJy beam^{-1}. The external thicker contour corresponds to the limit of detection of 2σ of the noise level for the combined continuum image (∼0.6 mJy beam^{-1}). Optical isophotal contour observed at the Gemini Telescope (grey) and elliptical fit (dashed line) are presented too.

Table 1. Main properties of the galaxies NGC 6907 and 6908. The index *opt* is for the optical observations (combining the g' and r' filters) and *rad* for the radio observations. *RA* and *Dec*. are the equatorial coordinates, V_0 the systemic velocity, a the size, i the inclination, *PA* the position angle, μ_B the surface brightness, *Type* the morphological type, D the galactocentric Hubble flow distance, $S_{\rm H\,I}$ the 21-cm flux density, A_B the Galactic extinction in B band, $V_{\rm max}$ the maximum velocity rotation, $r' - g'$ the colour in these filters, B the absolute B-band magnitude, L_B the total B luminosity, $M_{\rm dyn}$ the dynamical mass and $M_{\rm H\,I}/L_B$ the H I mass to B luminosity ratio. The number for the references are (1) Eskridge et al. (2002), (2) Madore et al. (2007) and (3) Amôres and Lépine (2005).

Parameters	NGC 6907	NGC 6908
RA (J2000)	$20^{\rm h}25^{\rm m}06\overset{\rm s}{.}63$	$20^{\rm h}25^{\rm m}08\overset{\rm s}{.}97$
Dec. (J2000)	$-24°48'33\overset{''}{.}0$	$-24°48'04\overset{''}{.}3$
V_0 (km s^{-1})	3182.4 ± 3.9	3147 ± 21
$a_{\rm opt}$ (arcsec)	90.0 ± 1.2	10.3 ± 0.6
$a_{\rm rad}$ (arcsec)	211.8 ± 1.9	–
$i_{\rm opt}$ (°)	31.1 ± 3.0	74.7 ± 3.1
$i_{\rm rad}$ (°)	46.4 ± 3.1	–
PA$_{\rm opt}$ (°)	76.4 ± 4.1	2.8 ± 1.4
PA$_{\rm rad}$ (°)	52.3 ± 11.5	–
μ_B	22.36 ± 0.05	20.81 ± 0.08
Type	SBbc[(1)]	S0(6/7)[(2)]
D (Mpc)	44.5 ± 3.1	43 ± 16
$S_{\rm H\,I}$ (mJy km s^{-1})	48.3 ± 1.8	–
A_B	0.12 ± 0.07[(3)]	0.12 ± 0.07[(3)]
$V_{\rm max}$ (km s^{-1})	215.8 ± 6.7	–
$r' - g'$	−1.55 ± 0.04	−1.50 ± 0.04
B	−21.69 ± 0.13	−17.43 ± 0.15
L_B(L$_\odot$)	(6.9 ± 1.3) × 10^{10}	(6.1 ± 0.9) × 10^8
$M_{\rm H\,I}$(M$_\odot$)	(8.3 ± 0.4) × 10^9	–
$M_{\rm dyn}$ (M$_\odot$)	(3.3 ± 0.4) × 10^{11}	–
$M_{\rm H\,I}/L_B$(M$_\odot$/L$_\odot$)	0.12 ± 0.01	–

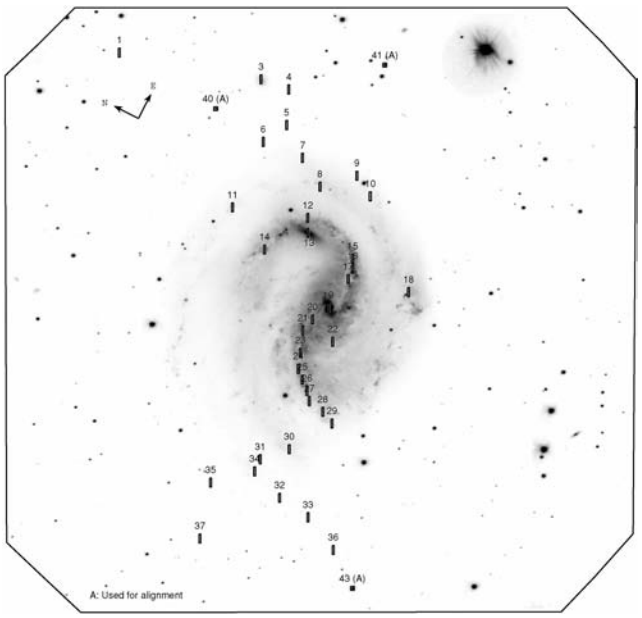

Figure 2. GMOS image of NGC 6907 in the g' filter overlapped by the representation of the slits. The slit 13 was used to sample NGC 6908 and the slit 19 to sample the optical centre of NGC 6907. Special squared slits signed with (A) were used to guarantee the alignment of the slits over the scientific targets.

As frequently happens, the MOS observations were broken in two stages: one for imaging and the other for spectroscopy. The images obtained in the first stage were employed to design the metallic mask with slits to perform the spectroscopy of the field and then used for photometric and morphological studies.

As required in the queue mode, a set of minimum conditions under which the observation could be executed were solicited. A minimum image quality of 70 per cent was requested and for this reason observations at 2×2 binned mode were chosen, shortening the readout time. As a compromise between spectral resolution and amount of light detected, all the slits were fixed with 1 arcsec widths. A standard slit height of 5 arcsec was chosen to improve the spatial sampling of the sky, since the typical source size of the candidates is almost 2 arcsec.

All the observations were executed in better conditions than required, ensuring full photometric conditions in all images. The seeing was 0.7 arcsec and the sky brightness was as good as 21.7 mag arcsec^{-2} in the g' filter and 20.1 mag arcsec^{-2} for the r' filter.

For all the observations, fast tip-tilt guiding was performed using wavefront sensors for image motion compensation. Only one on-instrument wavefront sensor (OIWFS) guide star (GSC0691101076) was needed for both imaging and spectroscopy observations.

Optical imaging for the NGC 6907 field was executed on 2005 August 1 using the filters g' (g_G0301) and r' (r_G0303). To guarantee a continuous coverage of the NGC 6907 field, we applied different dithering patterns to integrate a single frame in each filter.

The image files prepared in the first stage of the observations were used to select 33 H II region candidates over the NGC 6907 field, according to their brightness and geometry (Fig. 2). Standard procedures using the GMOS Mask Making Software were employed to design a mask with slits over each one of these candidates. A special slit was reserved for NGC 6908 (Slit 13).

The spectroscopic observations were carried out in 2005 September 2 in a single exposure of 960 s using the B600_G5303 grating. This disperser and the slit width of 1 arcsec guarantee a spectral resolution of ∼5 Å. No spectral dithering was used to cover the gaps on the final spectra, so special care was taken in choosing the central wavelength of 5000 Å by considering the systemic velocity of NGC 6907 and its expected rotation curve to avoid signal losses. The final spectra covered wavelengths between 3500 and 6300 Å. A CuAr arc lamp and a flat-field frame were observed in the sequence of the observation, while the telescope was still following the source, to guarantee the quality of the calibration frames, by avoiding any effect caused by torques over the instrument.

3.1 Data reduction procedures for Gemini observations

There are great differences for imaging and spectroscopy GMOS reduction, but for both cases the Gemini Data Reduction Software was used.

The reduction for images in filter g' and r' followed the same procedures. Individual dithered images of the field were corrected by overscan level, differences in gain for the detectors, bias and flat-field. After these steps, images from different detectors were mosaicked and all exposures were co-added in a clean image.

Spectroscopic data reduction requires some extra care. The first step was to prepare combined and normalized flat-field images, correcting this frame by overscan and bias. Since there was offsets between flat-field and the acquisition frames, the normalized flat-field was used for finding the slit edges using the gradient method. For this observation, an offset of six pixels in the spatial direction was applied.

Considering that a single frame was acquired in the spectroscopic observations, the cosmic rays could not be removed by combining frames. In this case, the task GSCRREJ was used. Residual effects on the spectral lines were corrected reprocessing only the slits affected by such correction, making the parameters for the cosmic ray removing more flexible.

An interactive process for the identification of spectral lines was set in each one of the analysed spectrum. Multiple solutions were obtained for the same spectrum using the spatial distribution of the spectral lines, improving the wavelength calibration.

For each slit, a local sky spectrum was extracted to be used to subtract the sky lines and continuum from the target spectrum. Standard sky lines were used to verify if there was raw systemic error in the observation.

After the visual inspection, the final spectra were generated by considering the on-source integrated emission in the spatial direction.

4 GMRT OBSERVATIONS

The interferometric mode of the GMRT was used for 21-cm imaging and spectroscopy. A more detailed description of this instrument is given by Swarup et al. (1991) and Ananthakrishnan & Pramesh Rao (2002).

The observations were carried out with a total baseband bandwidth of 4.0 MHz divided into 128 channels centred at 1405.40 MHz to cover the H I heliocentric velocity range of 2755–3610 km s^{-1} (optical definition). A summary of the main observational parameters is presented in Table 2.

The spectral resolution of the observation was 6.7 km s^{-1} per channel. Topocentric to heliocentric conversion of frequency was

Table 2. Observational parameters for the GMRT observation.

Parameter	Value
Date of observation	2006 July 13
Pointing centre (RA J2000)	$20^{\rm h}25^{\rm m}06\overset{\rm s}{.}652$
Pointing centre (Dec. J2000)	$-24^\circ48'33\overset{''}{.}492$
Observing duration (h)	4.7
Total on-source time (h)	2.6
Central frequency (MHz)	1405.40
Bandwidth per IF (MHz)	4.0
Number of spectral channels	128
Polarizations	2
Frequency resolution (kHz)	31.3
Velocity resolution (km s^{-1})	6.7
Flux calibrators	3C 48 and 3C 286
Phase calibrator	1923–210
Bandpass calibrator	3C 48, 3C 286 and 1923–210

done with the help of DOPSET task to take care of the Earth's motion at the date and time of observation.

The radio sources 3C 286 and 3C 48 were observed at the beginning and the end of the observation run as flux calibrator for ∼11 min each. VLA calibrator source 1923−210, which is an unresolved point source for GMRT (flux density of 2.0 Jy at 20 cm) was used as the phase calibrator. It was observed alternately for ∼5 min every ∼20 min observing NGC 6907.

4.1 Data reduction procedures for GMRT Observations

The radio data were reduced following standard calibration and imaging methods employing the classical AIPS. Flux densities at the observing frequency were estimated using the standard primary calibrators 3C 286 and 3C 48, also used to evaluate the flux densities and phases of the secondary calibrator. For 3C 286, the estimated flux density was 14.81 Jy and for 3C 48 it was 16.03 Jy. Taking into account the results of Omar et al. (2002) for 3C 48, the accuracy in the flux calibration must be better than 3 per cent. Since there was not any spectral features for 3C 48, 3C 286 and 1923−210 at the observing frequency, all of them were used to bandpass calibration.

Standard spectral line data reduction procedure was followed to remove bad data, to calibrate the gains and bandpass to produce the final calibrated visibilities for the target field.

A preliminary data cube was generated at spatial frequencies below 5 kλ to verify which channels would contain H I emission. Visual inspection, channel by channel, enabled us to register the detection of extended H I emission within the channels 41–105.

The polyhedron imaging technique was used to generate continuum images by averaging 42 line-free channels (ranging from 7 to 36 and 112 to 125), with data self-calibrated in both phase and amplitude. Spatial frequencies below 5 kλ were used and a Gaussian taper function was applied to weight down long baselines, reducing the sidelobes. In this case, the overall noise level was 2 mJy. The continuum flux density was subtracted from each individual channels and the final self-calibrated solutions were applied to the line-data to make an image cube with a resolution of 52×39 arcsec^2. To enhance the sensitivity to extended features, the data points were 'natural-weighted' and the resulting spectral cubes were cleaned for signals greater than 2.5 times the rms noise in the channel images.

To improve the spatial resolution for the analysis, several iterations of self-calibration were executed to make image cubes at different UV-ranges adapting the previous procedure.

Table 3. Parameters derived from the elliptical fitting to optical and radio isophotal data at 3σ of the sky or noise level; a and b are the major and minor axis of the ellipse, in arcsec, α_0 and δ_0 are the equatorial coordinates for the centre (J2000), i is the inclination, PA is the position angle, both in degrees.

Parameter	NGC 6907 Optical $\langle r'+g'\rangle$	NGC 6907 Radio (5 kλ)	NGC 6908 Optical $\langle r'+g'\rangle$
a	88.2 ± 1.8	212 ± 19	10.5 ± 0.8
b	77.4 ± 1.2	148 ± 10	3.2 ± 0.2
α_0	$20^{\rm h}25^{\rm m}06\overset{\rm s}{.}29$	$20^{\rm h}25^{\rm m}08\overset{\rm s}{.}70$	$20^{\rm h}25^{\rm m}08\overset{\rm s}{.}96$
δ_0	$-24^\circ48'16\overset{''}{.}3$	$-24^\circ48'43\overset{''}{.}6$	$-24^\circ48'03\overset{''}{.}4$
i	29.1 ± 4.2	46.4 ± 3.1	74.1 ± 4.5
PA	74.1 ± 6.6	52.3 ± 11.5	3.1 ± 2.1

The relationship between frequency and spectral-line velocity was set by means of the standard task ALTSWTCH. Moment maps were made from the resulting data cubes by using the AIPS task MOMNT (see the contours in Figs 6 and 9 for the zeroth and 1st moment map, respectively).

5 RESULTS

5.1 Optical photometry

The photometric calibration for the images in the filters g' and r' was made using the photometric standard stars in the MARK-A field (Landolt 1992), supplied by the Gemini baseline (GN-CAL20050611) and the usual procedures of the DAOPHOT IRAF tasks. Solutions including the atmospheric extinction were considered to determine the zero-point magnitudes for the g' ($m_0 = 31.72$) and r' ($m_0 = 31.60$). The results are in excellent agreement with the median atmospheric extinction coefficients for Mauna Kea, with differences lower than 0.4 per cent.

The limit of detection of the galaxies was taken as the 3σ limit of dispersion of the local sky level. For NGC 6907, these limits are 24.7 ± 0.2 mag arcsec^{-2} (g') and 23.6 ± 0.2 mag arcsec^{-2} (r'). For NGC 6908, they are 22.6 ± 0.3 and 21.4 ± 0.3 mag arcsec^{-2}, respectively, to the same filters.

Elliptical fittings in these isophotal limits, masked from the contribution of stellar fields, the interarm regions and the disturbed parts of the galaxy provided the projection parameters of NGC 6907 and 6908 (Table 3).

The integration of all flux inside these isophotes in each filter gives the g' and r' magnitudes. These values were converted to the standard B magnitude using the expressions by Fukugita et al. (1996) and Hook et al. (2004), corrected by the foreground Galactic extinction (Amôres and Lépine 2005) and masked from the foreground contributions. The results were a total B magnitude of 11.55 ± 0.03 and a mean effective surface brightness of 22.36 ± 0.05 mag arcsec^{-2} for NGC 6907 and a total B magnitude of 15.81 ± 0.15 and a mean effective surface brightness of 20.81 ± 0.08 mag arcsec^{-2} for NGC 6908.

The radial surface brightness profiles were obtained performing the integration of the flux on rings with the same size of the seeing (0.7 arcsec) and following the parameters of projection observed for the galaxy in each filter. For NGC 6907 (Fig. 3), the central variation of the brightness is compatible with a small spiral structure (usually identified as a bar) within (7.4 ± 2.1) arcsec. The exponential behaviour is only affected at radius near NGC 6908 emission, returning back to the exponential behaviour for larger distances. For NGC 6908, the surface brightness profiles are compatible with

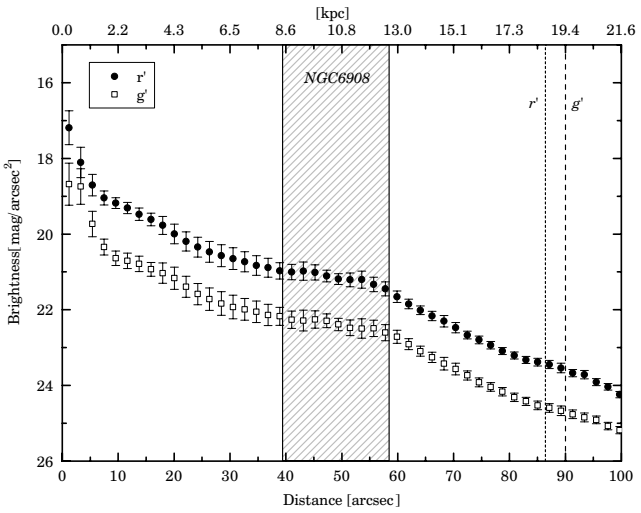

Figure 3. g' and r' radial surface brightness profiles. Special limits mentioned in the text are indicated by vertical or horizontal lines over the graph.

Madore et al. (2007), but the extended central emission of NGC 6908 suggests the presence of a composed nucleus.

5.2 Optical spectroscopy

For the spectrophotometric calibration, the sensitivity function was achieved using the flux standard star G191B2B supplied by the Gemini baseline, according to the specifications for the NGC 6907 spectral range coverage.

The IRAF package RVSAO was used to identify the spectral lines observed in the H II regions of NGC 6907 by cross-correlating a template spectrum of this kind of object to the observed spectra. A set of shifts and errors was determined for each spectral line and the radial velocities of all lines in each spectrum were combined by discarding the weakest lines and weighting the velocities with their errors and equivalent widths. The results of these processes are summarized in Table 4.

Special care was taken with the NGC 6908 spectrum (Fig. 4), since its optical depth is unknown and it can have contributions coming from NGC 6907 in its own spectrum. Taking into account that NGC 6908 is a lenticular S0 galaxy, then absorption lines must provide the most reliable information about its contents. Visual inspection was done to recognize spectral absorption lines and individual fitting profiles were performed considering Gaussian and Lorentzian models to obtain the central wavelength of the lines (see Table 5). Emission lines were detected inside the absorption lines, especially in the hydrogen lines (Fig. 5), confirming the spectra superposition.

5.3 Continuum

A more detailed view of the continuum emission of NGC 6907 shows a north-east elongated structure, with an asymmetric emission which does not provide good elliptical fitting (Fig. 1). The interaction between NGC 6907 and 6908 must be the main reason for such asymmetry. Almost all the continuum emission is confined to an isophote of 1.9 mJy beam^{-1} with approximately the same size than the optical emission centred at $\alpha_c = 20^{\rm h}25^{\rm m}07\overset{\rm s}{.}28$ and $\delta_c = -24^\circ 4' 33\overset{''}{.}9$. The total continuum flux measured for NGC 6907 is 112 mJy, in absolute agreement with Condon et al. (1998) and Vollmer et al. (2005), if the same isophotal limit is considered. The radial profile of this emission exhibits the expected behaviour for an exponential disc inside a de-projected radius of 72 arcsec.

Table 4. Observed radial velocities in direction of the selected H II regions in the optical ($v_{\rm opt}$) and in 21 cm ($v_{\rm H\,I}$). The ID is the slit number, *RA* and *Dec*. are the equatorial coordinates (J2000), r is the de-projected distance from the centre, considering the projection parameters of the radio for which the uncertainties are lower than 0.2 kpc ($H_0 = 73 \pm 5$ km/s/kpc).

ID	RA ($^{\rm h}$)	Dec. ($^\circ$)	r (kpc)	$v_{\rm H\,I}$ (km s^{-1})	$v_{\rm opt}$ (km s^{-1})
19	20.418508	−24.809166	0.8	3189 ± 92	3209 ± 10
20	20.418309	−24.807866	2.9	3234 ± 87	3182 ± 18
22	20.418197	−24.812122	4.5	3299 ± 32	3366 ± 28
21	20.418173	−24.807157	4.9	3224 ± 86	3181 ± 22
17	20.418904	−24.809892	5.6	3055 ± 56	3048 ± 9
16	20.418995	−24.810027	6.8	3098 ± 63	3136 ± 6
23	20.417903	−24.808552	7.7	3264 ± 62	3224 ± 11
15	20.419107	−24.809228	7.7	3055 ± 54	3123 ± 9
13	20.419157	−24.801142	8.8	3013 ± 37	3092 ± 52
24	20.417721	−24.809431	9.7	3295 ± 37	3350 ± 28
25	20.417622	−24.810875	10.7	3303 ± 31	3316 ± 11
12	20.419317	−24.799984	10.7	3000 ± 32	2948 ± 9
26	20.417594	−24.811851	10.9	3306 ± 30	3314 ± 20
14	20.418777	−24.796278	11.5	3044 ± 40	3062 ± 16
27	20.417468	−24.813068	12.4	3312 ± 25	3323 ± 11
28	20.417435	−24.815659	13.1	3315 ± 24	3363 ± 66
29	20.417363	−24.817730	14.3	3316 ± 23	3365 ± 25
08	20.419713	−24.799416	14.6	2996 ± 34	2982 ± 10
18	20.419087	−24.819066	14.9	3178 ± 37	3140 ± 5
10	20.419847	−24.807111	16.3	3045 ± 55	3081 ± 25
09	20.419967	−24.803985	17.2	3034 ± 55	2969 ± 26
11	20.419039	−24.788920	18.5	3041 ± 29	3024 ± 9
31	20.416655	−24.810240	22.9	3250 ± 21	3277 ± 19
34	20.416497	−24.810383	24.8	3240 ± 14	3263 ± 38
35	20.416154	−24.805107	31.0	3231 ± 15	3201 ± 20

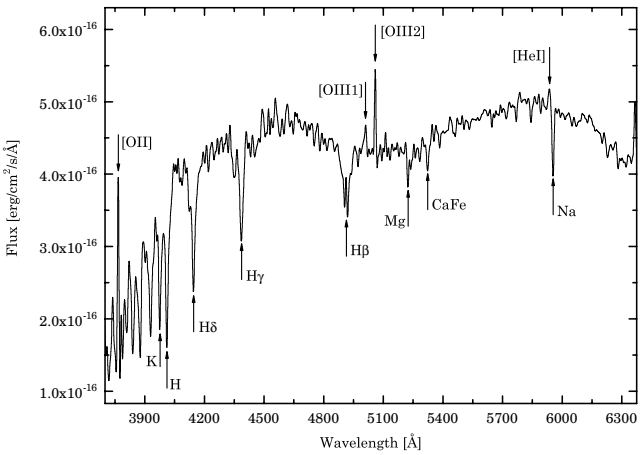

Figure 4. NGC 6908 integrated spectrum smoothed by removing Fourier components of higher frequencies. Absorption and emission lines are identified by the arrows.

5.4 H I emission

Subtracting the continuum image from the image cubes composed for UV ranges up to 40 kλ, it was possible to recover the spatial H I distribution for each channel, resolving structures larger than 10 × 12 arcsec. That is enough to sample the integrated contribution of the components inside the galaxy NGC 6907.

Table 5. Central wavelengths and velocities for the absorption spectral lines observed in direction of NGC 6908. λ_0 is the rest wavelength. λ_{abs} is the peak centroid and v_{abs} is the velocity associated to displacement of the observed spectral line.

Absorption line	λ_0 (Å)	λ_{abs} (Å)	v_{abs} (km s^{-1})
K	3933.70	3975.91 ± 0.36	3217 ± 13
H	3968.50	4011.31 ± 0.28	3234 ± 16
Hδ	4101.70	4145.49 ± 0.24	3201 ± 28
Hγ	4340.50	4386.68 ± 0.31	3189 ± 28
Hβ	4861.33	4914.56 ± 0.54	3283 ± 21
Mg	5175.36	5224.40 ± 0.28	2841 ± 17
CaFe	5268.98	5323.46 ± 0.49	3099 ± 21
Na	5892.50	5954.66 ± 0.25	3162 ± 33

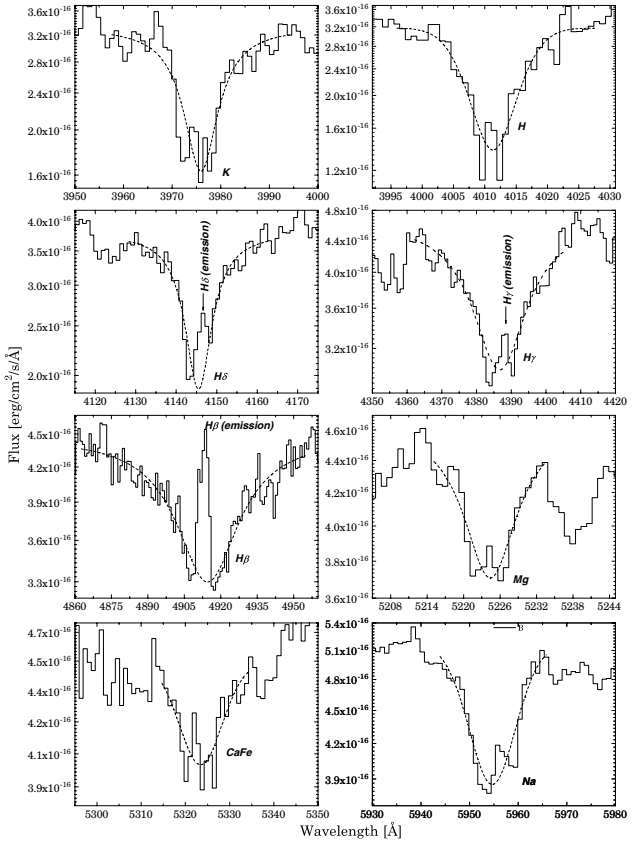

Figure 5. Detail of each absorption line (continuous line) and the fitted profile (dashed line). A Gaussian or Lorentzian profile was chosen depending on which minimizes the χ^2 per degree of freedom.

The bidimensional integration of the H I emission detected above 2σ of the noise level in all channels composes the zeroth moment. In Fig. 6, this map was converted to the H I column density assuming the relation by Spitzer (1978). It reveals a substantially more extended spiral structure than observed in optical images and the emission has two extended peaks coincident with the spiral arms.

Elliptical fitting for the isophote associated with a column density of 2.8×10^{19} cm^{-2} provides the extension of the radio emission as (3.5 ± 0.3) arcmin or almost 2.4 times larger than the optical emission (Table 3). Neither the optical centre nor the radio centre is coincident.

The integration of the column density on elliptical rings along NGC 6907 provides the radial column density profile presented in

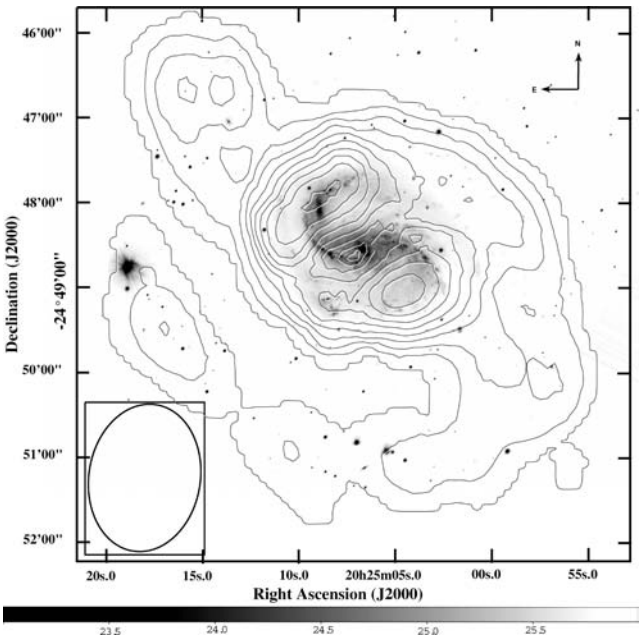

Figure 6. H I column density map over the g' image of NGC 6907 and 6908. The contour levels are at 0.3, 8.8, 17.3, 25.9, 34.4, 42.9, 51.4, 60.0, 68.5 and 77.0 in units of 10^{19} cm^{-2}.

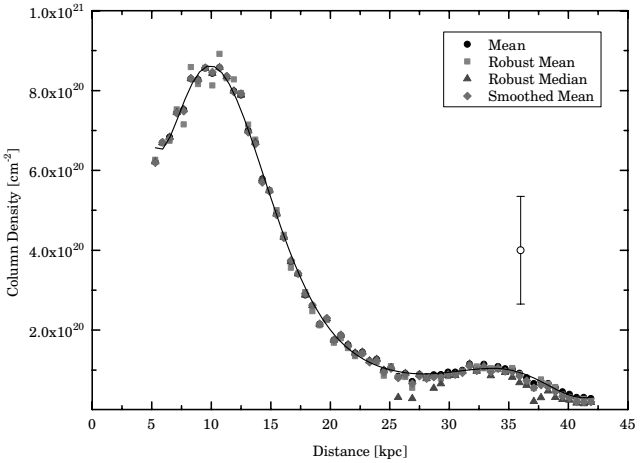

Figure 7. Radial H I column density profile. The open circle with error bars informs the mean error in data.

Fig. 7. As expected, there is a depletion of H I on the central regions of NGC 6907, since the molecular hydrogen is formed in a denser environments. After the peak emission at 10 kpc, an exponential fall occurs up to 28 kpc, where the column density rises up to 34 kpc and falls back again. Such distribution is quite common as can be seen in Broeils & van Woerden (1994), and the minimum inside the galactic disc can be related to the gas redistribution in the corotation radius.

On the other hand, the integration of all the emission for each channel of the data cube after continuum subtraction provides the global H I emission profile for the galaxies NGC 6907 and 6908 as it can be seen in Fig. 8.

The double-peaked emission is expected for rotating discs. Nevertheless, the different levels of the peaks indicate the presence of other components in the distribution of velocities measured in the field. These effects can be attributed to the spatial velocity of NGC 6908

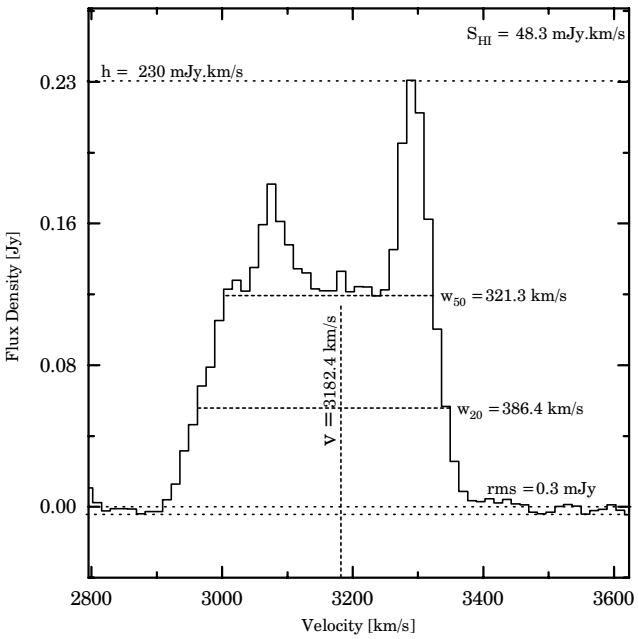

Figure 8. Global H I emission profile of NGC 6907 and 6908. The bottom dotted lines limit the noise level while the top dotted line indicates the maximum emission h. Inside the distribution, two horizontal dashed lines are used to mark the H I line-widths estimated at 20 per cent (w_{20}) and at 50 per cent (w_{50}) of the peak intensities; v is the central weighted mean velocity distribution.

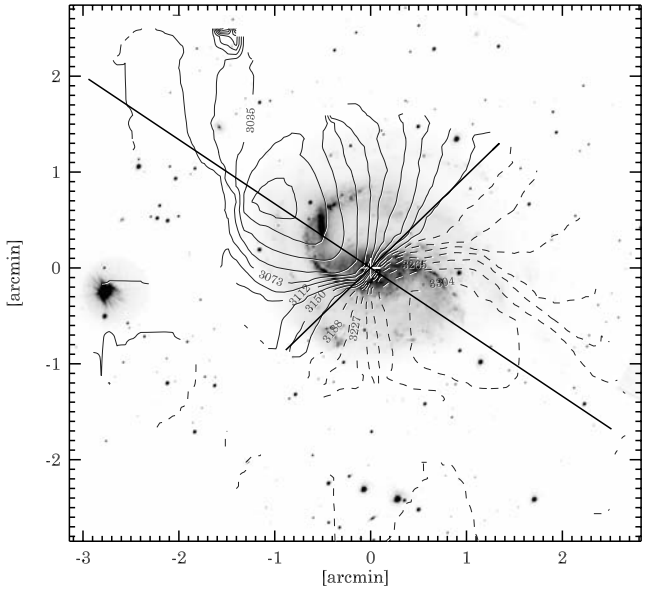

Figure 9. NGC 6907 velocity field superimposed over its image in g'. Dashed lines represent the part of the velocity field going away from the observer while the opposite is represented by the continuous lines. The thicker crossing lines represent the kinematical axis. The velocity field was generated using an UV range of 5 kλ and a resolution of 52×39 arcsec^2 to balance the sensitivity to the diffuse emission and the spatial resolution.

projected on the line-of-sight and to the intrinsic asymmetries on the velocity field of NGC 6907.

Richter & Huchtmeier (1991), Chengalur, Salpeter & Terzian (1993) and Doyle et al. (2005) observed these galaxies in lower resolution with different single dishes, what can possibly account for the main differences in the registered line profiles. The mean differences are lower than 3 per cent, including the flux density (48.3 ± 1.8 mJy km s^{-1}), suggesting that a beam smearing is mainly responsible for the differences found at the flux peak.

The weighted mean velocity associated with the H I profile (3182.4 ± 3.9 km/s) is absolutely compatible with the velocity measured by the robust mean of the entire first moment map (3183.2 ± 6.7 km s^{-1}). Taking into account the Hubble flow distance [supposing $H = (73 \pm 5)$ km s^{-1}Mpc^{-1}], the galactocentric distance of this galaxy is estimated as (44.5 ± 3.1) Mpc. Using this distance, a H I mass of $(8.3 \pm 0.4) \times 10^9$ M$_\odot$ was calculated.

Considering the distribution of velocities associated with the bidimensional emission in each frequency of the first moment map, the observed velocity field of the galaxy can be extracted (Fig. 9).

One can note that the velocity field is strongly oriented by the spiral arm in the internal regions. In fact, the high density of the H I emission in the spiral arms (from 10 to 100 times higher than the interarm regions) could generate a bias in the observed velocity field, if the velocity from the disc does not correspond to that measured in the spiral arms.

The kinematic major axis is not perpendicular to the kinematic minor axis (Fig. 9). That can be easily verified by comparing the linear fit over the coordinates of the points with the systemic velocity (minor axis) and the coordinates of the nearest points to the minor axis of all isovelocity levels, which samples the major axis in an axisymetric rotation disc. The angle between these axis is ($78\overset{\circ}{.}2 \pm 3\overset{\circ}{.}1$) and the point where they cross each other can be used to define the kinematic centre ($\alpha_k = 20^{\rm h}25^{\rm m}06\overset{\rm s}{.}40$ and $\delta_k = -24^\circ48'38\overset{''}{.}3$).

Since the global H I profile suggests that a rotating disc must be the main component of the movement of the system, the rotation curve of the galaxy NGC 6907 can be extracted supposing that the elliptical fitting made on the H I gas distribution represents the projection of the NGC 6907 disc on the sky and its gas follows circular orbits. In this situation, the observed line-of-sight velocity ignoring vertical and radial movements would be

$$v(\alpha, \delta) = V_0 + v_{\rm rot}(r, \theta)\sin(i)\cos(\theta) \quad (1)$$

taking into account that

$$\cos(\theta) = \frac{-(\alpha - \alpha_0)\sin(\phi)\cos(\delta) + (\delta - \delta_0)\cos(\phi)}{r} \quad (2)$$

$$\sin(\theta) = \frac{-(\alpha - \alpha_0)\cos(\phi)\cos(\delta) - (\delta - \delta_0)\sin(\phi)}{r\cos(i)} \quad (3)$$

where (α_0, δ_0) is the kinematic centre, V_0 is the systemic velocity, ϕ is the position angle of the receding semimajor axis, i is the inclination between the normal to the plane of the galaxy and the line-of-sight and r and θ are the polar coordinates inside the plane of the galactic disc.

Note that we introduce the term $\cos(\delta)$ multiplying all distances measured in right ascension (what it is not usually made in the literature), otherwise it would overestimate the galactocentric radius, depending on the declination of the source and the position angle of each target relative to the centre of the galaxy. For the NGC 6907, these errors are predominantly of the order of 12 per cent.

Using the combination of the velocity fields made with maps covering UV-ranges from 1 to 40 kλ, taking into account that the most reliable information about the rotation curve is extracted near the kinematic major axis ($\sim \pm 30^\circ$), then the previous equations can be used to determine $v_{\rm rot}$, r and θ for the receding and approaching regions of the galaxy (see Fig. 10). The tilted ring model was applied

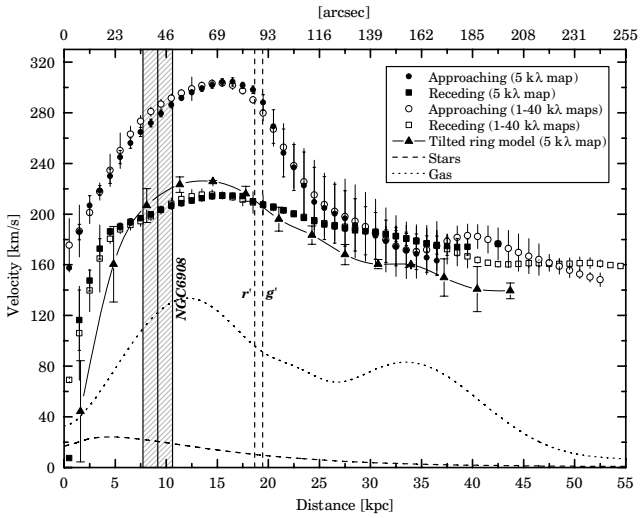

Figure 10. Rotation curves extracted for the receding and approaching regions of the NGC 6907 velocity field. The hatched area corresponds to the positions occupied by 6908 in the receding part of NGC 6907 and two vertical dashed lines represent elliptical fit limits in g' and r'. For the stellar rotation curve, it was supposed a mass-to-light ratio of 1.5.

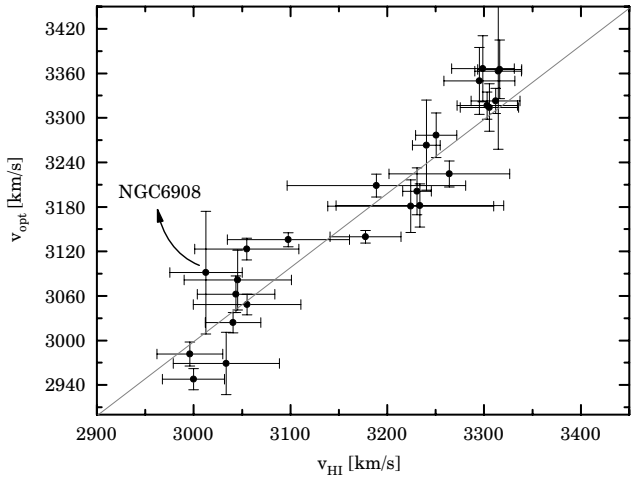

Figure 11. Comparison between optical radial velocities observed with GMOS and radio radial velocities observed with the GMRT. The straight continuous line represents the linear least-squares regression for the observed regions with azimuthal angles near the major axis ($\Delta\theta < 30^\circ$).

to the NGC 6907 velocity field, considering the same limits used in the previous method. Variations of the inclinations and the position angles with the distance are lower than the uncertainties for the position angle and inclination of the whole galaxy so its results can be ignored. A raw estimate for the dynamical mass of NGC 6907, considering the last point in the rotation curve, is $(3.3 \pm 0.9) \times 10^{11} M_\odot$.

Comparing the radial velocities from optical and H I spectra observed in the same directions (Fig. 11 and Table 4), it is possible to verify the overall correspondence between the optical and radio rotation curves [$v_{\rm opt} = (1.00 \pm 0.08) v_{\rm H\,I} + (1 \pm 240)$] and verify that the radio projection parameters provide the best correspondences. The high dispersion of individual points is related to the higher uncertainties to extract radial velocities azimuthaly far away from the major axis. In spite of that, the mean dispersion is inferior to the limit of 50 km s^{-1}, refereed by Bosma (1981) as the limit related to large-scale asymmetries of velocity fields. The exclusion of the objects at larger azimuthal angles relative to the major axis ($\Delta\theta = 30^\circ$) provides almost the same fit. In particular, the point representing the slit which sampled NGC 6908 presents a higher velocity dispersion than the others, possibly due to the spatial motion of NGC 6908.

6 DISCUSSION

A first view on the NGC 6907 velocity field (Fig. 9) reveals that NGC 6908 is over the approaching part of it. The extraction of the rotation curve in this part of the galaxy reveals contributions of radial components of the NGC 6908 movement, what does not occur in the receding part of the galaxy. This verification explains the different peak levels in the global H I emission profile shown in Fig. 8 and in the rotation curves presented in Fig. 10. Taking into account that the H I global profile preserves the behaviour expected for a rotating disc and different emission profiles agree with a exponential disc, then the effects of the interaction on the velocities can be considered as local. Consequently, the rotation curve extracted from the receding part of the velocity field is the real (undisturbed) NGC 6907 rotation curve.

Comparing the raw observed rotation curves from the receding and approaching parts of NGC 6907 in direction of NGC 6908, it is possible to see that the relative emission velocity between these galaxies (130 ± 17 km s^{-1}, as measured by Madore et al. 2007) coincides exactly with the expected velocity for the undisturbed rotation curve, and not with the velocity measured in radio for the approaching velocity field (where NGC 6908 can be found). This apparent contradiction can be easily understood considering that the emission line velocity measured for NGC 6908 is in fact from the rotating material in the NGC 6907 disc. NGC 6908, as a lenticular galaxy, has less gas and few new hot stars to heat it. So, the emission lines used by Madore to measure the NGC 6908 velocity only could come from the material in the NGC 6907 disc.

The idea that the emission lines come from the NGC 6907 is corroborated by the spectrum extracted in the direction of NGC 6908 (Fig. 4). It has a strong continuum superimposed by few emission lines, for which the radial velocity is (3092 ± 52) km s^{-1}, and by several absorption lines, associated to a radial velocity of (3147 ± 21) km s^{-1} (Table 5). Relative velocities spectroscopically measured in relation to the NGC 6907 centre (3209 ± 10 km s^{-1}) are 117 ± 53 km s^{-1} for emission lines (compatible with the NGC 6907 rotation curve in that direction) and (62 ± 23) km s^{-1} for absorption lines, in perfect agreement with Madore et al. (2007).

Another confirmation about the origin of the emission lines is that the broaden hydrogen absorption lines (typical of lenticular galaxies) contain vestiges of narrow emission lines inside it (Fig. 5). These emission lines have the same radial velocity of the rotation curve of NGC 6907 at that radius. That is the reason why different references and observations do not agree with the presence of certain hydrogen lines (they can be hidden in lower resolutions observations) and why Hβ is observed in absorption while Hα in emission. Since Hα line is more intense than Hβ, the equivalent absorption line formed in a different source is not deep enough to hide it.

Verifying the distribution of H I emission as a function of the velocity in the direction of NGC 6908, it is possible to distinguish three tied Gaussian components (Fig. 12). Considering the relative velocities measured with respect to the radio systemic velocity expected for the nucleus (since the spectrum extracted in the direction of the slit 19 does not sample the radio nucleus), the centroid of each component can be interpreted as associated with different structures in the interaction between NGC 6907 and 6908. The first one, at

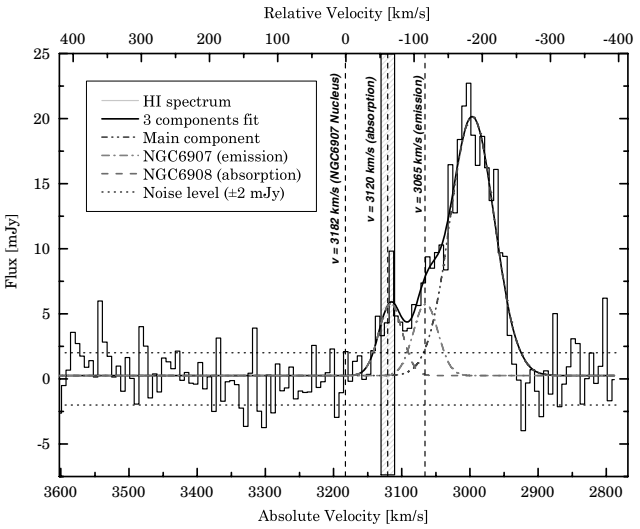

Figure 12. H I spectrum in the direction of NGC 6908 (grey stepped curve). The dashed vertical lines mark special velocities indicated in the picture. The horizontal dotted lines limit the noise level. Three components were fitted for this spectrum: the first associated with NGC 6908 by a dashed line, the second related to the NGC 6907 disc emission lines (dot–dashed line) and the third related to the gas left behind NGC 6908 due the interaction (dot-dot–dashed line). The sum of these components is represented by the smoothed black curve overlaying the observed H I profile (step grey line).

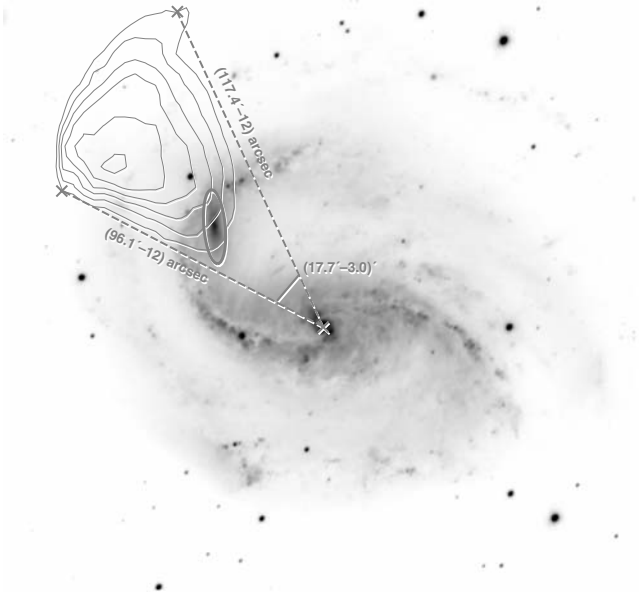

Figure 13. Contour of isovelocities higher than 220 km s^{-1} in the approaching region of the NGC 6907 velocity field overlaying the g' image of this galaxy. The interval between contours is 5 km s^{-1}.

3120 km s^{-1}, is associated with NGC 6908, since it has the same velocity of the absorption lines generated by its stellar content, the second one, at 3065 km s^{-1}, is produced by the excited material from the disc of NGC 6907 during the interaction with NGC 6908 and the third one (main component) related to the higher velocity gas left behind NGC 6908 due the interaction with NGC 6907.

6.1 A scenario for the collision between the two galaxies

Using the velocity contours above the approaching velocity of 220 km s^{-1}, it is possible to trace the disturbed regions of the velocity field and see a converging distribution of isophotes over NGC 6908, whose gradient is higher in direction of the rotation of NGC 6907, following the spiral arms (Fig. 13).

The striking triangular shape of the isophotes associated with high-velocity gas could be explained by the following scenario. NGC 6908 crossed the disc of NGC 6907 in a recent past, and very probably the tidal forces created a bridge of gas between the two galaxies, similar to the Magellanic stream in our galaxy. The gas left behind NGC 6908 disc by the collision explains the excess of gas approaching us. In our galaxy, at the solar Galactic radius, the time required for a gas cloud launched in the direction perpendicular to the plane to revert its motion and fall back on to it is about 35 Myr (see e.g. Lépine & Duvert 1994). This can be taken as an order of magnitude for the present case. Let us now consider the velocity component of NGC 6908 in the plane of the sky. This component is directed approximately towards the centre of NGC 6907, as we can infer from the fact that presently NGC 6908 is situated closer to the centre of NGC 6907 than the marks left in the gas of the disc by the crossing event. The gas stream produced by the collision must also have a component of velocity in the same (almost radial) direction, which explains why the triangular isophotes point towards NGC 6908. Finally, let us analyse the component of velocity of the stream in the plane of the sky, but in the direction of rotation of NGC 6907. The stream can, in a simplified way, be considered as a mixture of gas with velocities ranging from that of NGC 6908 (with almost zero component in the direction of rotation of NGC 6907) to the gas which resulted to have about the same rotation velocity of the disc of NGC 6907. This explains the elongated shape of the isophotes in the direction of rotation, and at the same time, allows us to estimate in a new way the time elapsed since the collision. The mean de-projected distance of the two extremes of the gas with perturbed velocity in Fig. 13 is about (104.8 ± 17.9) arcsec, where the undisturbed rotation curve has the velocity of (200.0 ± 6.7) km s^{-1}. Assuming $H_0 = (73 \pm 5)$ km s^{-1}Mpc, this distance is (22.6 ± 4.1) kpc. Since the angle between the two extremes is ($17\overset{\circ}{.}7 \pm 0\overset{\circ}{.}3$), the initial disturbed material would have travelled (7.0 ± 1.2) kpc azimuthally. From this we derive that the collision occurred about (3.4 ± 0.6) × 10^7 yr ago, which is consistent with the order of magnitude previously estimated.

7 CONCLUSIONS

The combination of the GMRT radio observation and GMOS/Gemini optical observation provides a more complete view about the interaction between the galaxies NGC 6907 and 6908.

Photometric images observed at the Gemini Telescope and the H I maps observed at the GMRT reveal extended structures that can be understood as tidal debris in optical images, but resemble the continuation of the spiral arms in radio. By fitting ellipses to the last isophotes registered to each one of these observations for NGC 6907, we verified that the 21-cm emission is 2.4 times more extended than the optical emission. The orientation of the fitted ellipses provides different parameters of projection for optical and radio observations, the differences being $15\overset{\circ}{.}3$ for the inclination and $24\overset{\circ}{.}1$ for the position angle. Geometric, photometric and kinematic centres are not coincident, reinforcing the evidences about the effect of an interaction in NGC 6907.

The spectra observed using the GMOS spectrograph are coherent with those observed in 21 cm in the same direction of the slits. The

parameters of projection in radio provide the best correspondences between the optical and radio velocities. The details of the emission and absorption lines observed in direction of NGC 6908 show that they have different origins. First, because the observed emission lines are not typical of lenticular galaxies like [O II] (3727 Å), [O III] (4959 and 5007 Å) and the He I (5876 Å), especially for those with low luminosity like NGC 6908. Secondly, because the radial velocity observed in absorption is different from the velocity emission lines, which are coherent with the undisturbed rotation curve of NGC 6907 expected for that direction. Finally, because inside the hydrogen absorption lines it is possible to see traces of narrower hydrogen recombination lines with a Doppler effect suitable for the NGC 6907 rotating disc, confirming their different origin.

The H I column density distribution presents a discontinuity in its radial profile which can be related to the gas redistribution at the corotation radius. The details of the global H I emission profile reveals that the rotation is the main component of the H I velocity distribution, and its asymmetry indicates the contribution of the NGC 6908 motion is local and in velocities near to those found in the NGC 6907 rotating disc. The total H I mass obtained was $(8.3 \pm 0.4) \times 10^9$ $M_\odot$.

Due to the dominant contribution to the H I emission in the spiral arms, they can be the main contributors for the velocity field asymmetries, verified by the non-perpendicularity of the kinematic axis (difference of 12°).

The differences in the rotation curve extracted from the receding and approaching parts of the velocity field can be interpreted as the consequence of line-of-sight components produced by the interaction with NGC 6908. Assuming that the interaction only affected the side where NGC 6908 is observed in projection, and that the velocity field of the opposite side is the real rotation curve of NGC 6907, we were able to get a raw estimate for the dynamical mass of $(3.3 \pm 0.4) \times 10^{11}$ $M_\odot$.

Looking at the H I spectrum in the direction of NGC 6908, it is possible to distinguish three emission components: one coincident with the relative velocity for NGC 6908, another coincident with the excited gas in NGC 6907 disc and the last one in agreement with the higher relative velocities gas left behind NGC 6908 by dynamic friction. Using the difference in the rotation curves extracted from the disturbed region of the velocity field and that one away from this region, we found the limits for the disturbed material on the NGC 6907. Supposing that this material has drifted inside the NGC 6907 disc, according the rotation curve, we estimated the time when the interaction started in $(3.4 \pm 0.6) \times 10^7$ yr.

Another work is in preparation to discuss the metallicity distribution in the NGC 6907 and its possible connection with the corotation radius.

ACKNOWLEDGMENTS

We thank the staff of the GMRT that made these observations possible. GMRT is run by the National Centre for Radio Astrophysics of the Tata Institute of Fundamental Research. Financial support for this work was provided by Conselho Nacional para o Desenvolvimento Científico e Tecnológico (CNPq) and Coordenação de Aperfeiçoamento Pessoal de Nível Superior (CAPES). This research has benefited by the NASA's Astrophysics Data System (ADS) and Extra-galactic Data base (NED) services. Their open software used in this research is greatly acknowledged. The Gemini programme ID for the data used in this paper is the GN-2005B-Q-39 (PI:S. Scarano Jr). We thank C. Mendes de Oliveira and Jayaram N. Chengalur for the helpful discussions.

REFERENCES

Amôres E. B., Lépine J. R. D., 2005, AJ, 130, 659
Ananthakrishnan S., Pramesh Rao A., 2002, The Giant Metrewave Radio Telescope. Mumbai Ebenezer Printing House, Mumbai, p. 233
Bosma A., 1981, AJ 86, 1825
Broeils A. H., van Woerden H., 1994, A&AS, 107, 129
Chengalur J. N., Salpeter E. E., Terzian Y., 1993, ApJ, 419, 30
Condon J. J., Cotton W. D., Greisen E. W., Yin Q. F., Perley R. A., Taylor G. B., Broderick J. J., 1998, AJ, 115, 1693
Doyle M. T. et al., 2005, MNRAS, 361, 34
Eskridge P. B. et al., 2002, ApJS, 143, 73
Fillmore J. A., Boroson T. A., Dressler A., 1986, ApJ, 302, 208
Fukugita M., Ichikawa T., Gunn J. E., Doi M., Shimasaku K., Schneider D. P., 1996, AJ, 111, 1748
Garcia A. M., 1993, A&AS, 100, 47
García-Barreto J. A., Franco J., Carrillo R., Venegas S., Escalante-Ramírez B., 1996, Rev. Mex. Astron. Astrofis., 32, 89
García-Barreto J. A., Carrillo R., Vera-Villamizar N., 2003, AJ, 126, 1707
Hook I. M., Jørgensen I., Allington-Smith J. R., Davies R. L., Metcalfe N., Murowinski R. G., Crampton D., 2004, PASP, 116, 425
Kormendy J., Westpfahl D. J., 1989, ApJ, 338, 752
Landolt A. U., 1992, AJ, 104, 340
Lauberts A., Valentijn E. A., 1989, The Surface Photometry Catalogue of the ESO-Uppsala Galaxies. European Southern Observatory, Garching
Lépine J. R. D., Duvert G., 1994, A&A, 286, 60
Madore B. F., Gil de Paz A., Pevunova O., Thompson I., 2007, AJ, 134, 314
Maia M. A. G., da Costa L. N., Latham D. W., 1989, ApJS, 69, 809
Omar A., Dwarakanath K. S., Rupen M., Anantharamaiah K. R., 2002, A&A, 394, 405
Pizzella A., Corsini E. M., Vega Beltrán J. C., Bertola F., 2004, A&A, 424, 447
Rhee G., Valenzuela O., Klypin A., Holtzman J., Moorthy B., 2004, ApJ, 617, 1059
Richter O.-G., Huchtmeier W. K., 1991, A&AS, 87, 425
Saito M., Sasaki M., Kaneko N., Nishimura M., Toyama K., 1984, PASJ, 36, 305
Spitzer L., 1978, Physical Processes in the Interstellar Medium. Wiley-Interscience, New York, p. 333
Surace J. A., Sanders D. B., Mazzarella J. M., 2004, AJ, 127, 3235
Swarup G., Ananthakrishnan S., Kapahi V. K., Rao A. P., Subrahmanya C. R., Kulkarni V. K., 1991, Curr. Sci., 60, 95
Vega Beltrán J. C., Pizzella A., Corsini E. M., Funes J. G., Zeilinger W. W., Beckman J. E., Bertola F., 2001, A&A, 374, 394
Vollmer B., Davoust E., Dubois P., Genova F., Ochsenbein F., van Driel W., 2005, VizieR Online Data Catalog, 8074

This paper has been typeset from a TEX/LATEX file prepared by the author.